Dalton Transactions

ROYAL SOCIETY OF CHEMISTRY

PAPER

View Article Online
View Journal

Cite this: DOI: 10.1039/d6dt00929h

Aromatic guest-induced layer expansion and phase switching in a 2D square lattice coordination network

Shi-Qiang Wang, *[a] Shaza Darwish, [b] Shan Xu,[a] Rong Wang *[a] and Michael J. Zaworotko *[b]

Switching coordination networks (CNs) that exhibit guest-induced phase transformations hold promise for molecular recognition and separation, yet their responsiveness to different adsorbates remains underexplored. Herein, we further investigate the previously reported guest-induced layer expansion and phase switching behavior of a 2D square lattice (**sql**) topology CN, $[Co(4,4'\text{-bipyridine})_2(NCS)_2]_n$ (**sql-1-Co-NCS**), in the presence of a new group of aromatic guests, methylbenzene (MB), nitrobenzene (NB), and 1,3,5-trimethylbenzene (TMB). Overall, aromatic guest-induced open phases can be classified into three categories based on the number of guest molecules accommodated per formula unit, **H·*x*G** (*x* = 2, 3, 4), with interlayer distances spanning 5.92–9.61 Å. The TMB-loaded phase is unusual as it exhibits an alternating layered arrangement with two distinct interlayer distances of 8.29 and 8.80 Å. Vapor adsorption studies of **sql-1-Co-NCS** revealed that MB vapor triggers phase switching at a lower relative pressure than C_8 aromatics, indicating a stronger host framework response and highlighting the potential of this material for the separation of substituted benzene derivatives.

Received 22nd April 2026,
Accepted 2nd May 2026

DOI: 10.1039/d6dt00929h

rsc.li/dalton

Introduction

Switching coordination networks (CNs) represent a fascinating and growing class of soft porous crystals or flexible metal–organic frameworks (FMOFs) that can undergo reversible structural transformations between "closed" nonporous and "open" porous phases induced by external stimuli such as temperature, pressure, light, or guest molecules.[1–9] This dynamic behaviour, often referred to as breathing or gate-opening, is not just a curiosity as it offers potential applications in gas storage, hydrocarbon separation, sensing, and catalysis.[10–16]

A key factor governing the gate-opening behaviour of switching CNs is the interaction between the host framework and guest molecules.[17–19] Guest species, ranging from gases to vapours and liquids, can induce structural transformations of the host framework through noncovalent interactions such as hydrogen bonding, van der Waals forces, C–H···π contacts, and π–π stacking. Understanding these host–guest interactions is therefore crucial, as they directly influence the gate-opening threshold pressure, adsorption capacity, and selectivity of switching CNs.

However, precisely determining the locations and binding sites of guest molecules in switching CNs remains challenging. As-synthesised crystals often lose their single crystallinity upon activation, while the degree of framework flexibility is significantly influenced by the nature of guest molecules, frequently resulting in guest-loaded phases that differ from the as-synthesised phase. Although *in situ* characterization techniques such as coincident gas sorption and *in situ* X-ray diffraction (XRD) can partially address this issue,[20–24] accurate structural determination remains difficult, especially when an appropriate template structure is unavailable.

Aromatic solvents are widely used in MOF synthesis, and some of them, including toluene and xylenes, also serve as important chemical feedstocks so their separation and purification are of relevance. One approach to gain insight into guest–framework interactions is to exploit different aromatic solvents during MOF synthesis, which can yield either identical or distinct structures containing various inclusion solvent molecules.[25] In recent years, we have investigated the adsorption properties of two-dimensional (2D) square lattice (**sql**) CNs $[M(bpy)_2(A)_2]$ (bpy = 4,4′-bipyridine; M = Fe, Co, or Ni, A = NCS; M = Cu, A = BF_4 or CF_3CO_2), **sql-1-M-A**, with respect to a range of adsorbates including N_2, CH_4, CO_2, C_2H_2, C_2H_4, C_2H_6, C_3H_4, C_3H_6, C_3H_8, H_2O, and xylenes.[26–34] Their switching behavior typically results in stepped or sigmoidal adsorption isotherms that depend on the metal centre, terminal anion, temperature and/or adsorbate. In particular, their ability to separate

[a]*Singapore Membrane Technology Centre, Nanyang Environment and Water Research Institute, Nanyang Technological University, 1 Cleantech Loop, 637141, Singapore. E-mail: shiqiang.wang@ntu.edu.sg, rwang@ntu.edu.sg*
[b]*Bernal Institute, Department of Chemical Sciences, University of Limerick, Limerick V94 T9PX, Republic of Ireland. E-mail: xtal@ul.ie*

xylene isomers provides a counterintuitive strategy for addressing challenging hydrocarbon separations.[27,28,34] These findings prompted us to study the effect of a broader range of aromatic adsorbates on **sql-1-M-NCS** by means of single-crystal X-ray diffraction (SCXRD) and vapor adsorption measurements, in order to further elucidate their guest-dependent phase switching behaviour.

Results and discussion

Single crystals of $\{[M(bpy)_2(NCS)_2]\cdot xG\}_n$ (**sql-1-M-NCS·*x*G**, M = Co, G = nitrobenzene (NB) and 1,3,5-trimethylbenzene (TMB); M = Fe, G = methylbenzene (MB)) were synthesized by solvent diffusion using a procedure similar to that previously reported for G = α,α,α-trifluorotoluene (TFT), *o*-xylene (OX), *m*-xylene (MX), *p*-xylene (PX), and ethylbenzene (EB).[26,27] SCXRD measurements (Table S1) reveal that both **sql-1-Co-NCS·2NB** and **sql-1-Fe-NCS·2MB** crystallize in the monoclinic space group *C*2/*c*, whereas **sql-1-Co-NCS·3TMB** adopts the triclinic space group $P\bar{1}$. Despite crystallographic differences, all three structures retain **sql** topology in which each metal center is linked equatorially by bpy ligands and axially by two terminal NCS ligands, as observed in the TFT-, OX-, MX-, PX-, and EB-loaded phases.[26,27] Powder X-ray diffraction (Fig. S1) and thermogravimetric analysis (Fig. S2) of **sql-1-Co-NCS·2NB** confirm the bulk phase purity and thermal stability of the network up to 175 °C.

Based on the structural parameters summarized in Table 1, the aromatic guest-induced phase transformations of **sql-1-M-NCS** can be classified according to the number of guest molecules accommodated per formula unit, **H·*x*G** (*x* = 2, 3, 4). For smaller aromatic guests such as MB, EB, NB, and TFT, the network incorporates two guest molecules per formula unit, **H·2G**, including **sql-1-Fe-NCS·2MB**, **sql-1-Co-NCS·2EB**, **sql-1-Co-NCS·2NB** and **sql-1-Co-NCS·2TFT**. Compared with the closed parent phase, **sql-1-Co-NCS**,[26,35] which exhibits square grid angles of 75.3/104.7° and an interlayer distance of 4.46 Å, guest inclusion induces moderate expansion of the interlayer distance of networks (Fig. 1). In addition, the square grid angles become more orthogonal (*ca.* 85.6–87.9°/92.1–94.4°), while the ∠Co–N–CS hinge angles decrease to 149.6–157.8°, indicating a hinge-like

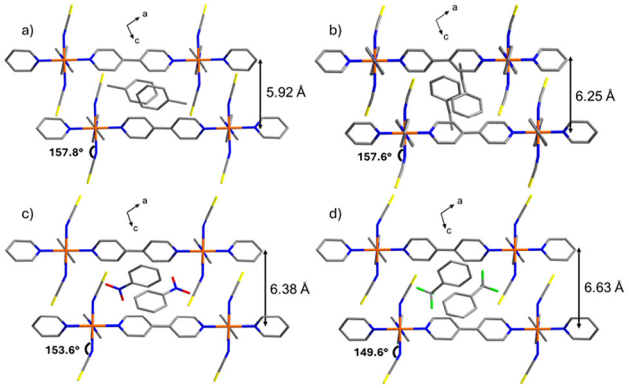

Fig. 1 Crystal structures of (a) MB-, (b) EB-, (c) NB-, and (d) TFT-loaded phases. H atoms are omitted for clarity. Co: brown; N: blue; C: grey; S: yellow; O: red; F: green.

bending associated with gate-opening. Correspondingly, the interlayer distance increases to 5.92–6.63 Å and the calculated void fraction rises to 38.0–43.7%. Both parameters follow the trend MB < EB < NB < TFT, consistent with their molecular weights (Table S2). The bpy ligands remain 50% coplanar and 50% twisted, with torsion angles ranging from 37.8–57.4°, indicating that guest inclusion also influences the degree of local framework distortion.

A distinct structural response is observed for TMB, which induces formation of **sql-1-Co-NCS·3TMB** with three guest molecules per formula unit (**H·3G**). This structure exhibits an unusual alternating layered arrangement with two distinct interlayer distances of 8.29 and 8.80 Å (Fig. 2). These correspond to two different hinge conformations defined by ∠Co–N–CS angles of 159.2° and 175.1°, respectively. The more bent hinge angle (159.2°) leads to a relatively compressed interlayer distance of 8.29 Å (designated as type A), whereas the nearly linear hinge angle (175.1°) corresponds to a larger interlayer distance of 8.80 Å (type B). Consequently, the framework adopts an alternating ABAB layered structure with a calculated void of 60.2%. The three TMB guest molecules occupy distinct regions of the structure: one resides within the square grid cavity, while the other two are located in the type A and type B interlayer spaces, respectively. This rare structural arrangement

Table 1 Structural parameters of **sql-1-M-NCS** and its aromatic guest-loaded phases

Compound	Square grid angles (°)	$\angle_{Co-N-CS}$ (°)	bpy torsion angle[b] (°)	Interlayer distance (Å)	Void[c] (%)
sql-1-Co-NCS (100 K)[26]	75.3/104.7	170.9	50% (54.5); 50% coplanar	4.46	0
sql-1-Fe-NCS·2MB (100 K)[a]	86.6/93.4	157.8	50% (47.4); 50% coplanar	5.92	38.0
sql-1-Co-NCS·2EB (100 K)[27]	87.9/92.1	157.6	50% (51.4); 50% coplanar	6.25	40.5
sql-1-Co-NCS·2NB (273 K)[a]	86.5/93.5	153.6	50% (37.8); 50% coplanar	6.38	41.7
sql-1-Co-NCS·2TFT (273 K)[26]	85.6/94.4	149.6	50% (43.6); 50% coplanar	6.63	43.7
sql-1-Co-NCS·3TMB (100 K)[a]	88.4/91.6	159.2/175.1	50% (34.1); 50% (35.3)	8.29/8.80	60.2
sql-1-Co-NCS·4PX (100 K)[27]	90/90	160.3	50% (39.9); 50% coplanar	9.15	64.7
sql-1-Co-NCS·4MX (100 K)[27]	89.3/90.7	162.8	100% (32.6)	9.21	64.1
sql-1-Co-NCS·4OX (100 K)[27]	90/90	166.1	50% (29.3); 50% coplanar	9.26	63.7

[a] This work. [b] Coplanarity is defined herein as a torsion angle <2°. [c] Probe radius = 1.2 Å.

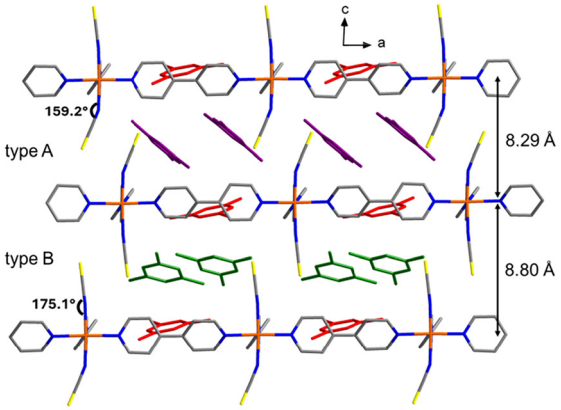

Fig. 2 Crystal structure of **sql-1-Co-NCS·3TMB**. H atoms are omitted for clarity. The three crystallographically independent TMB molecules are highlighted in red, purple, and green, respectively.

highlights the adaptability of the 2D **sql** CNs to accommodate bulky aromatic guests through cooperative hinge flexibility and layer expansion.

For the xylene isomers, the network incorporates four guest molecules per formula unit (**H·4G**) to form phases **sql-1-Co-NCS·4C$_8$H$_{10}$** (C$_8$H$_{10}$ = PX, MX, and OX). As described in our previous work,[27] in these phases the square grid angles approach an ideal square geometry (~90/90°), and the ∠Co–N–CS hinge angles increase to 160.3–166.1°. The interlayer distance expands further to 9.15–9.26 Å at 100 K, while the void fraction reaches 63.7–64.7%. Our recent study further revealed that at 303 K the xylene-loaded phases exhibit interlayer distances of 9.46–9.61 Å with void fraction of 65.1–66.0%.[32,36] These phases correspond to the largest layer expansion of **sql-1-M-A** reported to date (Fig. 3 and Table S3),[37–50] further demonstrating the structural adaptability of the network in response to aromatic guest inclusion.

Interestingly, adaptive structural rearrangements of the host network induced by different aromatic guests affords distinct channel architectures (Fig. 4): 2D channels for the **H·2G** phases; 3D channels for the TMB/xylene-loaded phases. In the **H·2G** structures, the 2D channel is divided into two equal segments because of the staggered packing of adjacent layers, as exemplified by **sql-1-Co-NCS·2NB** (Fig. 4a and d). The NB molecules reside in these channel segments, similar to the arrangement observed in **sql-1-Cu-CF$_3$CO$_2$·2OX**.[34] The 3D channel of **sql-1-Cu-CF$_3$CO$_2$·3TMB** features a nearly square channel in which three pairs of TMB molecules are accommodated (Fig. 4b and e). The xylene-loaded phases also display 3D channels, but with a rhombic geometry, as exemplified by **sql-1-Co-NCS·4PX**, where two pairs of PX molecules occupy the channel (Fig. 4c and f).

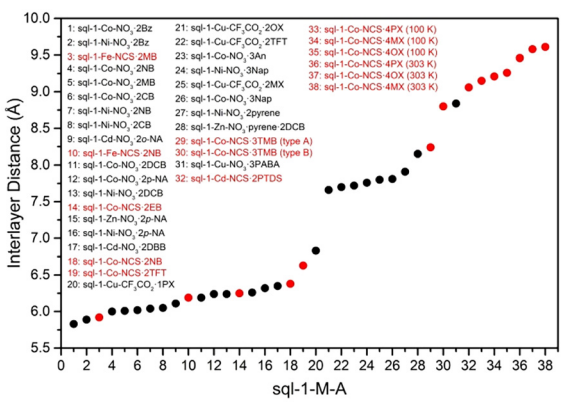

Fig. 3 Summary of aromatic guest-induced interlayer distances for **sql-1-M-A** reported to date. Red circles indicate members of the **sql-1-M-NCS** family.

These different crystal packing patterns are accompanied by distinct host–guest interactions. For the xylene-loaded phase, the host–guest and guest–guest interactions have been discussed in our previous work.[27,32,36] For the **H·2G** phases, as demonstrated by **sql-1-Co-NCS·2NB** (Fig. 5a), the NB molecule is located in an ordered position within the interlayer space thanks to multiple weak interactions with adjacent networks. A π···π interaction (3.854 Å) is observed between the aromatic ring of NB and the pyridyl ring of the bpy ligand. In addition, a relatively short C–H···O hydrogen bond (2.605 Å) involves the nitro group and two C–H···π interactions (3.116 and 3.363 Å) occur between the NB molecule and bpy ligands. A C–H···S contact (2.964 Å) is observed between an aromatic C–H moiety of NB and the S atom of the NCS ligand. These weak interactions anchor the NB molecules within the interlayer space and sustain the layer-expanded structure.

For **sql-1-Co-NCS·3TMB**, three crystallographically independent TMB molecules (colored red, purple, and green in Fig. 2) exhibit distinct host–guest interactions. The red TMB located within the square grid cavity (Fig. 5b) interacts primarily through C–H···π interactions between the methyl C–H groups and the pyridyl rings, with distances of 2.771–3.193 Å. The purple TMB molecule (Fig. 5c) which is situated in the type A compressed interlayer region engages in four C–H···π interactions (2.600, 2.911, 3.169, and 3.457 Å) and one C–H···S contact (3.294 Å). The green TMB molecule (Fig. 5d) that lies in the type B interlayer region participates in extensive host–guest and guest–guest interactions, including four C–H···π contacts (2.494, 2.972, 3.255, and 3.441 Å) and four C–H···S contacts (3.045, 3.168, 3.266, and 3.375 Å). These interactions form a supramolecular network that links adjacent layers, thereby stabilizing the expanded structure and preserving alternating expanded interlayer distance observed in the TMB-loaded structure.

Vapor adsorption measurements (Fig. 6) provided insight into the phase switching behavior of **sql-1-Co-NCS**. Although TFT can induce the formation of **sql-1-Co-NCS·2TFT** under solvent diffusion conditions, its vapor did not open the closed parent phase, **sql-1-Co-NCS**, over the measured pressure range. In contrast, MB vapor triggered gate opening at ~16% P/P_0, with a saturation uptake reaching 38.0 wt% at 90% P/P_0. This adsorption capacity corresponds to two MB molecules per formula unit (2 mol mol^{-1}, Fig. S3), consistent with the crystallographic data for **sql-1-Fe-NCS·2MB**. Moreover, the lower gate-

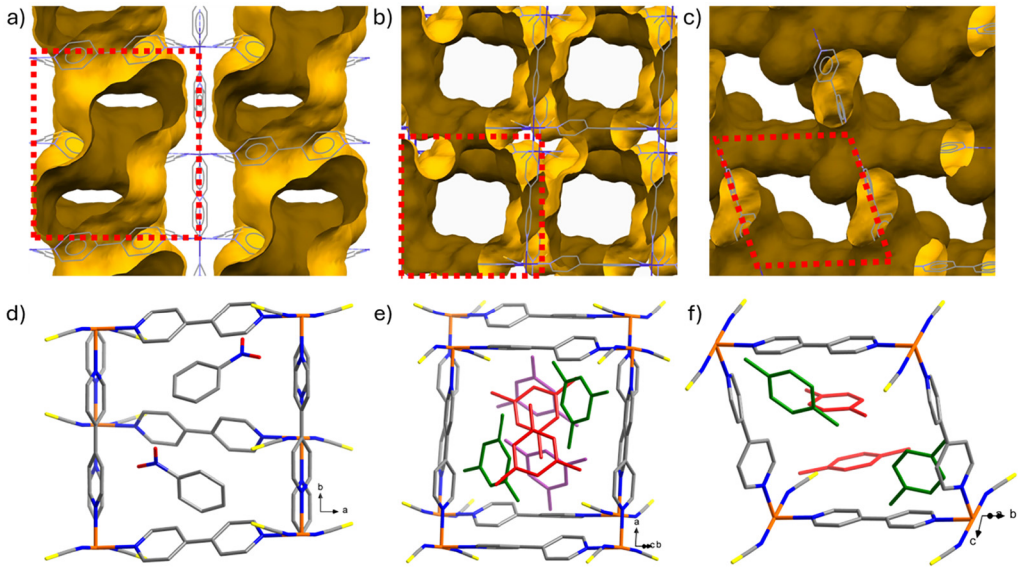

Fig. 4 Channel profiles (a–c) and the corresponding enlarged view (d–f) of the red dash line regions for **sql-1-Co-NCS·2NB**, **sql-1-Co-NCS·3TMB**, and **sql-1-Co-NCS·4PX**, respectively.

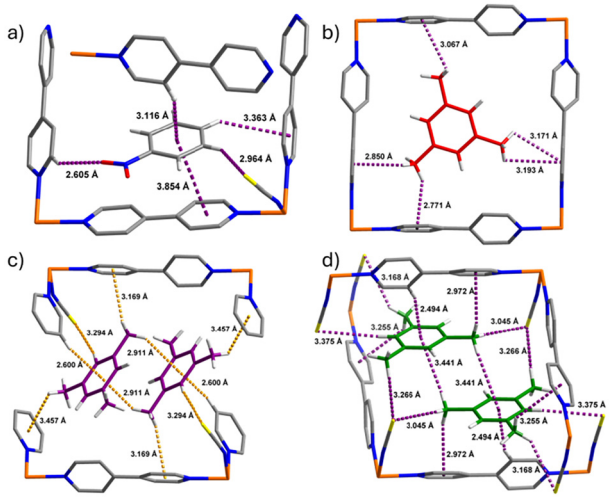

Fig. 5 Host–guest interactions for (a) **sql-1-Co-NCS·2NB**, and (b–d) **sql-1-Co-NCS·3TMB**, respectively.

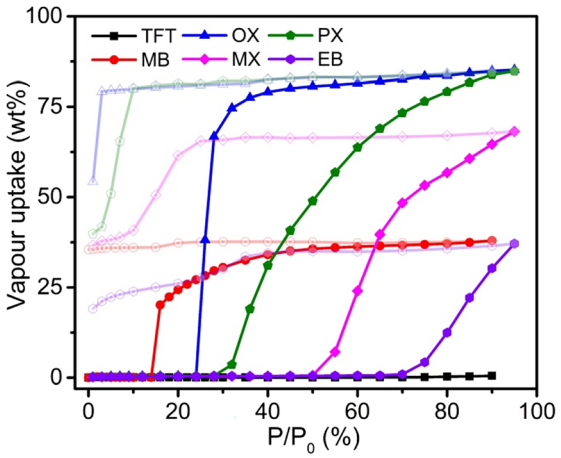

Fig. 6 Vapor adsorption isotherms (298 K) of **sql-1-Co-NCS**. Adsorption: solid symbols; desorption: open symbols.

opening pressure of MB compared with those of the C_8 aromatics reported previously indicates potential applicability of this material for the separation of substituted benzene derivatives.[27] These behaviours can be attributed to differences in the driving force arising from host–guest interactions.[7] In addition, our previous studies have demonstrated that guest adsorption–desorption in **sql-1-Co-NCS** is reversible and recyclable,[26,27] and that intermediate phases may exist even though they are not detectable in sorption isotherms.[24] Furthermore, a metal-center effect has previously been observed in CO_2 adsorption and is expected to also play a role in aromatic guest adsorption,[30] which merits further investigation.

Conclusions

In summary, **sql-1-Co-NCS** exhibits guest-dependent layer expansion and phase switching between closed (guest-free) and open (guest-loaded) structures. Aromatic guests differing in functional groups (methyl, ethyl, nitro, and trifluoromethyl) as well as the number and substitution position of methyl groups induce distinct open phases with varied interlayer distances, void fractions, and host–guest or guest–guest interactions. Although flexible CNs/MOFs have been explored for guest-induced structural transformations, this study adds to our understanding of how the shape, size, and functionalization of aromatic guests influence the phase transformation

behavior of 2D switching CNs. The combination of structural flexibility and selective guest responsiveness highlights **sql-1-M-NCS** as a promising platform for hydrocarbon separations and offers insights for the design of stimuli-responsive materials. Ongoing studies will further explore the adsorption behavior of additional aromatic guests in this family of 2D switching CNs.

Experimental section

Synthesis of sql-1-M-NCS·*x*G

In a typical procedure, 4,4′-bipyridine (0.3 mmol, 46.8 mg) was dissolved in 5 mL of an aromatic solvent (NB, MB, or TMB) to form the bottom layer. A mixture of ethanol (2.5 mL) and the corresponding aromatic solvent (2.5 mL) served as the buffer layer. A solution of $Co(NCS)_2$ (0.15 mmol, 26.3 mg) in 5 mL of ethanol was then carefully layered on top of the buffer layer. The layered solution was left undisturbed for several days to yield the target crystals. It should be noted that direct synthesis of **sql-1-Co-NCS·2MB** using this method was unsuccessful. Instead, **sql-1-Fe-NCS·2MB** was prepared using the same solvent diffusion method, except that the top layer was replaced with a solution of $FeSO_4{\cdot}7H_2O$ (0.15 mmol, 41.7 mg) and NaSCN (0.3 mmol, 24.3 mg) dissolved in 5 mL of ethanol. One entry of its single-crystal structural data (refcode: QAGWAY) has been reported previously.[48]

Single-crystal X-ray diffraction measurements

Suitable single crystals of all compounds were chosen for single-crystal X-ray diffraction measurements. Data were collected on a Bruker D8 Quest diffractometer equipped with a IμS microfocus Cu anode (λ = 1.54178 Å) and Photon II detector. In all cases, data were indexed, integrated and scaled in APEX3. Absorption correction was performed by a multi-scan method. Space groups were determined using XPREP implemented in APEX3. Structures were solved using the intrinsic phasing method (SHELXT) and refined on F^2 using full-matrix least-squares techniques with SHELXL contained in OLEX2 v1.2.8. All non-hydrogen atoms were refined anisotropically. Hydrogen atoms were located in idealized positions based on molecular geometry and assigned isotropic displacement parameters tied to those of their carrier atoms.

Crystallographic data for the as-synthesized **sql** CNs are summarized in Table S1. All crystal structures have been deposited with the Cambridge Crystallographic Data Centre (CCDC 2543884–2543886).

Powder X-ray diffraction

Powder X-ray diffraction experiment was conducted using microcrystalline samples on a Panalytical Empyrean diffractometer (40 kV, 40 mA, Cu Kα1,2, λ = 1.5418 Å). A scan speed of 0.111747° s^{-1} (6.7° min^{-1}), with a step size of 0.026° in 2θ was used at room temperature with a range of 5° < 2θ < 40°.

Thermogravimetric analysis (TGA)

TGA was carried out under N_2 atmosphere in a TA instruments Q50 thermal analyzer between room temperature and 600 °C with a constant heating rate of 10 °C min^{-1}.

Vapor sorption experiments

TFT and MB vapor adsorption measurements were conducted using a Surface Measurement Systems DVS Vacuum following a procedure similar to that previously reported for C8 aromatic isomers.[27] Approximately 10 mg of **sql-1-Co-NCS** was degassed *in situ* under vacuum (1×10^{-4} Torr), and vapor adsorption was then measured by stepwise increasing the relative pressure from 0 to 90%, with equilibration at each step determined by the sample weight change criterion (dM/dT = 0.01% min^{-1}).

Author contributions

Shi-Qiang Wang: methodology, investigation, formal analysis, funding acquisition, writing – original draft; Shaza Darwish: investigation, writing – review & editing; Shan Xu: writing – review & editing; Rong Wang: funding acquisition, writing – review & editing; Michael J. Zaworotko: supervision, funding acquisition, writing – review & editing.

Conflicts of interest

There are no conflicts to declare.

Data availability

The data supporting this article have been included as part of the supplementary information (SI). Supplementary information: TGA curves, PXRD patterns, adsorption isotherms, *etc*. See DOI: https://doi.org/10.1039/d6dt00929h.

CCDC 2543884–2543886 contain the supplementary crystallographic data for this paper.[51a–c]

Acknowledgements

S.-Q. W. acknowledges support from A*STAR under the Manufacturing, Trade and Connectivity (MTC) Young Individual Research Grant (M24N8c0105). Rong Wang and Shan Xu acknowledge support from the National Research Foundation, Singapore, and Agency for Science, Technology and Research (A*STAR) under its RIE 2025 Urban Solutions and Sustainability (USS) Low Carbon Energy Research (LCER) Phase 2 Programme 1st Emerging Technology Grant Call (ETGC) (Award: U2411D4007). M. J. Z. acknowledges the support of Research Ireland (16/IA/4624, 21/US/3760).

References

1 S. Horike, S. Shimomura and S. Kitagawa, Soft porous crystals, *Nat. Chem.*, 2009, **1**, 695–704.
2 A. Schneemann, V. Bon, I. Schwedler, I. Senkovska, S. Kaskel and R. A. Fischer, Flexible metal-organic frameworks, *Chem. Soc. Rev.*, 2014, **43**, 6062–6096.
3 Z. Chang, D.-H. Yang, J. Xu, T.-L. Hu and X.-H. Bu, Flexible Metal-Organic Frameworks: Recent Advances and Potential Applications, *Adv. Mater.*, 2015, **27**, 5432–5441.
4 J.-P. Zhang, H.-L. Zhou, D.-D. Zhou, P.-Q. Liao and X.-M. Chen, Controlling flexibility of metal–organic frameworks, *Natl. Sci. Rev.*, 2018, **5**, 907–919.
5 S. Krause, N. Hosono and S. Kitagawa, Chemistry of Soft Porous Crystals: Structural Dynamics and Gas Adsorption Properties, *Angew. Chem., Int. Ed.*, 2020, **59**, 15325–15341.
6 F. Bigdeli, C. T. Lollar, A. Morsali and H.-C. Zhou, Switching in Metal–Organic Frameworks, *Angew. Chem., Int. Ed.*, 2020, **59**, 4652–4669.
7 S.-Q. Wang, S. Mukherjee and M. J. Zaworotko, Spiers Memorial Lecture: Coordination Networks that Switch between Nonporous and Porous Structures: An Emerging Class of Soft Porous Crystals, *Faraday Discuss.*, 2021, **231**, 9–50.
8 J. Dong, V. Wee and D. Zhao, Stimuli-responsive metal–organic frameworks enabled by intrinsic molecular motion, *Nat. Mater.*, 2022, **21**, 1334–1340.
9 I. Senkovska, V. Bon, L. Abylgazina, M. Mendt, J. Berger, G. Kieslich, P. Petkov, J. Luiz Fiorio, J.-O. Joswig, T. Heine, L. Schaper, C. Bachetzky, R. Schmid, R. A. Fischer, A. Pöppl, E. Brunner and S. Kaskel, Understanding MOF Flexibility: An Analysis Focused on Pillared Layer MOFs as a Model System, *Angew. Chem., Int. Ed.*, 2023, **62**, e202218076.
10 G. Férey and C. Serre, Large breathing effects in three-dimensional porous hybrid matter: facts, analyses, rules and consequences, *Chem. Soc. Rev.*, 2009, **38**, 1380–1399.
11 J. H. Lee, S. Jeoung, Y. G. Chung and H. R. Moon, Elucidation of flexible metal-organic frameworks: Research progresses and recent developments, *Coord. Chem. Rev.*, 2019, **389**, 161–188.
12 B. Qian, Z. Chang and X. H. Bu, Functionalized Dynamic Metal-Organic Frameworks as Smart Switches for Sensing and Adsorption Applications, *Top. Curr. Chem.*, 2019, **378**, 5.
13 D.-D. Zhou and J.-P. Zhang, On the Role of Flexibility for Adsorptive Separation, *Acc. Chem. Res.*, 2022, **55**, 2966–2977.
14 K. Koupepidou, A. Subanbekova and M. J. Zaworotko, Functional flexible adsorbents and their potential utility, *Chem. Commun.*, 2025, **61**, 3109–3126.
15 F. Xie, F.-A. Guo, H. Wang and J. Li, Flexible metal-organic frameworks for hydrocarbon separations, *Coord. Chem. Rev.*, 2025, **541**, 216831.
16 I. Senkovska, V. Bon, A. Mosberger, Y. Wang and S. Kaskel, Adsorption and Separation by Flexible MOFs, *Adv. Mater.*, 2025, **37**, e2414724.
17 P. L. Llewellyn, P. Horcajada, G. Maurin, T. Devic, N. Rosenbach, S. Bourrelly, C. Serre, D. Vincent, S. Loera-Serna, Y. Filinchuk and G. Ferey, Complex adsorption of short linear alkanes in the flexible metal-organic-framework MIL-53(Fe), *J. Am. Chem. Soc.*, 2009, **131**, 13002–13008.
18 N. A. Ramsahye, T.-K. Trung, S. Bourrelly, Q.-Y. Yang, T. Devic, G. Maurin, P. Horcajada, P. L. Llewellyn, P. Yot, C. Serre, Y. Filinchuk, F. Fajula, G. Ferey and P. Trens, Influence of the Organic Ligand Functionalization on the Breathing of the Porous Iron Terephthalate Metal Organic Framework Type Material upon Hydrocarbon Adsorption, *J. Phys. Chem. C*, 2011, **115**, 18683–18695.
19 S.-Q. Wang, S. Darwish and M. J. Zaworotko, Adsorbate-dependent phase switching in the square lattice topology coordination network $[Ni(4,4'\text{-bipyridine})_2(NCS)_2]_n$, *Chem. Commun.*, 2023, **59**, 559–562.
20 J.-P. Zhang, P.-Q. Liao, H.-L. Zhou, R.-B. Lin and X.-M. Chen, Single-crystal X-ray diffraction studies on structural transformations of porous coordination polymers, *Chem. Soc. Rev.*, 2014, **43**, 5789–5814.
21 V. Bon, E. Brunner, A. Pöppl and S. Kaskel, Unraveling Structure and Dynamics in Porous Frameworks via Advanced In Situ Characterization Techniques, *Adv. Funct. Mater.*, 2020, **30**, 1907847.
22 S. Bureekaew, H. Sato, R. Matsuda, Y. Kubota, R. Hirose, J. Kim, K. Kato, M. Takata and S. Kitagawa, Control of Interpenetration for Tuning Structural Flexibility Influences Sorption Properties, *Angew. Chem., Int. Ed.*, 2010, **49**, 7660–7664.
23 K. Koupepidou, V. I. Nikolayenko, D. Sensharma, A. A. Bezrukov, M. Shivanna, D. C. Castell, S.-Q. Wang, N. Kumar, K.-i. Otake, S. Kitagawa and M. J. Zaworotko, Control over Phase Transformations in a Family of Flexible Double Diamondoid Coordination Networks through Linker Ligand Substitution, *Chem. Mater.*, 2023, **35**, 3660–3670.
24 S.-Q. Wang, V. Bon, S. Darwish, S.-M. Wang, Q.-Y. Yang, Z. Xu, S. Kaskel and M. J. Zaworotko, Insight into the Gas-Induced Phase Transformations in a 2D Switching Coordination Network via Coincident Gas Sorption and In Situ PXRD, *ACS Mater. Lett.*, 2024, **6**, 666–673.
25 F. Millange, C. Serre, N. Guillou, G. Ferey and R. I. Walton, Structural effects of solvents on the breathing of metal-organic frameworks: an in situ diffraction study, *Angew. Chem., Int. Ed.*, 2008, **47**, 4100–4105.
26 S.-Q. Wang, Q.-Y. Yang, S. Mukherjee, D. O'Nolan, E. Patyk-Kazmierczak, K.-J. Chen, M. Shivanna, C. Murray, C. C. Tang and M. J. Zaworotko, Recyclable switching between nonporous and porous phases of a square lattice (sql) topology coordination network, *Chem. Commun.*, 2018, **54**, 7042–7045.
27 S.-Q. Wang, S. Mukherjee, E. Patyk-Kaźmierczak, S. Darwish, A. Bajpai, Q.-Y. Yang and M. J. Zaworotko, Highly Selective, High-Capacity Separation of *o*-Xylene from

C8 Aromatics by a Switching Adsorbent Layered Material, *Angew. Chem., Int. Ed.*, 2019, **58**, 6630–6634.

28 N. Kumar, S.-Q. Wang, S. Mukherjee, A. A. Bezrukov, E. Patyk-Kaźmierczak, D. O'Nolan, A. Kumar, M.-H. Yu, Z. Chang, X.-H. Bu and M. J. Zaworotko, Crystal engineering of a rectangular sql coordination network to enable xylenes selectivity over ethylbenzene, *Chem. Sci.*, 2020, **11**, 6889–6895.

29 S.-Q. Wang, X.-Q. Meng, M. Vandichel, S. Darwish, Z. Chang, X.-H. Bu and M. J. Zaworotko, High Working Capacity Acetylene Storage at Ambient Temperature Enabled by a Switching Adsorbent Layered Material, *ACS Appl. Mater. Interfaces*, 2021, **13**, 23877–23883.

30 S.-Q. Wang, S. Darwish, D. Sensharma and M. J. Zaworotko, Tuning the switching pressure in square lattice coordination networks by metal cation substitution, *Mater. Adv.*, 2022, **3**, 1240–1247.

31 S.-Q. Wang, S. Darwish, X.-Q. Meng, Z. Chang, X.-H. Bu and M. J. Zaworotko, Acetylene storage performance of [Ni (4,4′-bipyridine)$_2$(NCS)$_2$]$_n$, a switching square lattice coordination network, *Chem. Commun.*, 2022, **58**, 1534–1537.

32 E. Patyk-Kaźmierczak, M. Kaźmierczak, S.-Q. Wang and M. J. Zaworotko, Pressure-Induced Structural Effects in the Square Lattice (sql) Topology Coordination Network sql-1-Co-NCS·4OX, *Cryst. Growth Des.*, 2023, **23**, 2055–2064.

33 S.-Q. Wang, S. Darwish and M. J. Zaworotko, The impact of solution vs. slurry vs. mechanochemical syntheses upon the sorption performance of a 2D switching coordination network, *Inorg. Chem. Front.*, 2023, **10**, 3821–3827.

34 S.-Q. Wang, C. R. M. O. Matos, S. Darwish, V. Bon, Y. Luo, J. Zhu, X. Zhang, Z. Xu, S. Kaskel and M. J. Zaworotko, Guest-Induced Phase Switching in a Square Lattice Coordination Network to Enable Selective Adsorption of p-Xylene, *ACS Appl. Mater. Interfaces*, 2025, **17**, 39183–39190.

35 M. Wriedt and C. Näther, Preparation of New Ligand-Deficient Thiocyanato Compounds with Cooperative Magnetic Phenomena by Thermal Decomposition of Their Ligand-Rich Precursors, *Eur. J. Inorg. Chem.*, 2010, **2010**(20), 3201–3211.

36 S.-Q. Wang and M. J. Zaworotko, Structural Insights into Exceptional Layer Expansion and *o*-Xylene Selectivity of a 2D Switching Coordination Network, *Chem. – Eur. J.*, 2026, submitted.

37 M. Fujita, Y. J. Kwon, S. Washizu and K. Ogura, Preparation, clathration ability, and catalysis of a two-dimensional square network material composed of cadmium(II) and 4, 4′-bipyridine, *J. Am. Chem. Soc.*, 1994, **116**, 1151–1152.

38 S. Huang, B. Lewandowski, C. Liu and Y. Shan, [Cd (4, 4′-bipy)$_2$(NO$_3$)$_2$](2-nitroaniline)$_2$, a novel two-dimensional lattice inclusion compound, *Acta Crystallogr., Sect. C:Cryst. Struct. Commun.*, 1999, **55**, 2016–2018.

39 K. Biradha, K. V. Domasevitch, C. Hogg, B. Moulton, K. N. Power and M. J. Zaworotko, Interpenetrating covalent and noncovalent nets in the crystal structures of [M(4,4′-bipyridine)$_2$(NO$_3$)$_2$] 3C$_{10}$H$_8$ (M = Co, Ni), *Cryst. Eng.*, 1999, **2**, 37–45.

40 K. Domasevitch and M. Zaworotko, Covalent and noncovalent interpenetrating planar networks in the crystal structure of {[Ni (4, 4′-bipyridine)$_2$(NO$_3$)$_2$ 2pyrene}n, *Chem. Commun.*, 1999, 1327–1328.

41 K. Biradha, A. Mondal, B. Moulton and M. J. Zaworotko, Coexisting covalent and non-covalent planar networks in the crystal structures of {[M(bipy)$_2$(NO$_3$)$_2$]·arene}n (M = Ni, 1; Co, 2; arene = chlorobenzene, o-dichlorobenzene, benzene, nitrobenzene, toluene or anisole), *J. Chem. Soc., Dalton Trans.*, 2000, (21), 3837–3844.

42 K. Biradha, A. Mondal, B. Moulton and M. J. Zaworotko, Coexisting covalent and non-covalent planar networks in the crystal structures of {[M(bipy)$_2$(NO$_3$)$_2$]·arene}n (M = Ni, 1; Co, 2; arene = chlorobenzene, o-dichlorobenzene, benzene, nitrobenzene, toluene or anisole), *J. Chem. Soc., Dalton Trans.*, 2000, 3837–3844.

43 B. Moulton, E. Rather and M. Zaworotko, Interpenetration of covalent and noncovalent networks in the crystal structures of {[M (4, 4′-bipyridine)$_2$(NO$_3$)$_2$]·2p-nitroaniline}n where M= Co, 1, Ni, 2, Zn, 3, *Cryst. Eng.*, 2001, **4**, 309–317.

44 A. Kondo, H. Noguchi, S. Ohnishi, H. Kajiro, A. Tohdoh, Y. Hattori, W.-C. Xu, H. Tanaka, H. Kanoh and K. Kaneko, Novel expansion/shrinkage modulation of 2D layered MOF triggered by clathrate formation with CO2 molecules, *Nano Lett.*, 2006, **6**, 2581–2584.

45 A. Kondo, H. Noguchi, L. Carlucci, D. M. Proserpio, G. Ciani, H. Kajiro, T. Ohba, H. Kanoh and K. Kaneko, Double-Step Gas Sorption of a Two-Dimensional Metal-Organic Framework, *J. Am. Chem. Soc.*, 2007, **129**, 12362–12363.

46 G. J. McManus, J. J. Perry IV, M. Perry, B. D. Wagner and M. J. Zaworotko, Exciplex Fluorescence as a Diagnostic Probe of Structure in Coordination Polymers of Zn2+ and 4, 4′-Bipyridine Containing Intercalated Pyrene and Enclathrated Aromatic Solvent Guests, *J. Am. Chem. Soc.*, 2007, **129**, 9094–9101.

47 X.-L. Yang, S.-B. Ren, J. Zhang, Y.-Z. Li, H.-B. Du and X.-Z. You, Syntheses and structures of three coordination polymers based on 4-methylbenzenethiolates of Zn(II) and Cd(II) and bipyridine, *J. Coord. Chem.*, 2009, **62**, 3782–3794.

48 C. J. Adams, J. A. Real and R. E. Waddington, The two-dimensional iron(II)-thiocyanate-4,4′-bipyridine coordination network, *CrystEngComm*, 2010, **12**, 3547–3553.

49 H. Kajiro, A. Kondo, K. Kaneko and H. Kanoh, Flexible two-dimensional square-grid coordination polymers: structures and functions, *Int. J. Mol. Sci.*, 2010, **11**, 3803–3845.

50 A. Kondo, S.-i. Noro, H. Kajiro and H. Kanoh, Structure- and phase-transformable coordination polymers/metal complexes with fluorinated anions, *Coord. Chem. Rev.*, 2022, **471**, 214728.

51 (*a*) CCDC 2543884: Experimental Crystal Structure Determination, 2026, DOI: 10.5517/ccdc.csd.cc2rd3s2; (*b*) CCDC 2543885: Experimental Crystal Structure Determination, 2026, DOI: 10.5517/ccdc.csd.cc2rd3t3; (*c*) CCDC 2543886: Experimental Crystal Structure Determination, 2026, DOI: 10.5517/ccdc.csd.cc2rd3v4.